IEEE Access
Multidisciplinary | Rapid Review | Open Access Journal

Received 18 February 2025, accepted 2 April 2025, date of publication 10 April 2025, date of current version 22 April 2025.

Digital Object Identifier 10.1109/ACCESS.2025.3559722

RESEARCH ARTICLE

Coordinated Control of Flywheel and Battery Energy Storage Systems for Frequency Regulation in Diesel Generator-Based Microgrid

MAHDI FARAJI[1], MOHAMMAD SAEED MAHDAVI[2], VENERA NURMANOVA[3], GEVORK B. GHAREHPETIAN[1], (Senior Member, IEEE), AND MEHDI BAGHERI[3], (Senior Member, IEEE)

[1]Department of Electrical Engineering, Amirkabir University of Technology (AUT), Tehran 15916-34311, Iran
[2]Department of Electrical Engineering, Isfahan University of Technology, Isfahan 84156-83111, Iran
[3]Department of Electrical and Computer Engineering, School of Engineering and Digital Sciences, Nazarbayev University, Astana 010000, Kazakhstan

Corresponding author: Mehdi Bagheri (mehdi.bagheri@nu.edu.kz)

This work was supported in part by the Faculty Development Competitive Research Grant (FDCRG), Nazarbayev University, under Grant 201223FD8811; and in part by the Collaborative Research Project (CRP), Nazarbayev University, under Grant 211123CRP1604.

ABSTRACT Due to the inherent slow response time of diesel generators within an islanded microgrid (MG), their frequency and voltage control systems often struggle to effectively manage rapid load changes. To mitigate this challenge, energy storage systems (ESSs) emerge as pivotal solutions. Flywheel energy storage systems (FESSs) are well-suited for handling sudden power fluctuations because they can quickly deliver or absorb large amounts of electricity. On the other hand, battery energy storage systems (BESSs) excel at storing large amounts of energy for extended periods and can handle gradual changes in power demand. This research introduces a coordinated control mechanism for a mixed energy storage setup that combines BESS and FESS elements to manage the frequency of a standalone MG. A new frequency detection method is employed to assign high, medium, and low-frequency deviations in power distribution to FESS, BESS, and diesel generators, respectively. Simulations are carried out to determine the exact performance of the proposed control method. The MATLAB/Simulink software platform is used to run these simulations. Furthermore, dynamic load changes are precisely emulated using a programmable load emulator enhancing the reliability and relevance of our analysis.

INDEX TERMS Microgrid, flywheel energy storage system, battery energy storage system, diesel generator emulator, frequency regulation.

NOMENCLATURE

BESS	Battery Energy Storage System.
BPF	Band pass filter.
DG	Distributed generation.
DGE	Diesel generator emulator.
DER	Distributed Energy Resources.
FESS	Flywheel Energy Storage System.
FIR	Finite Impulse Response.
FOC	Field Oriented Control.
HE	High energy.
HESS	Hybrid energy storage system.
HP	High power.
HPF	High pass filter.
LE	Load emulator.
LPF	Low pass filter.
MG	Microgrid.
MPPT	Maximum power point tracking.

The associate editor coordinating the review of this manuscript and approving it for publication was Lei Wang.

PSO	Particle swarm optimization.
PWM	Pulse width modulation.
SLD	Single line diagram.
SMES	Super-conducting magnetic energy storage Systems.
THD	Total harmonic distortion.

NOTATIONS

A(z)	Transfer function of FIR filter.
Apass	Passband Ripple.
Astop	Stopband Attenuation.
$Astop1$	Lower Stopband Attenuation.
$Astop2$	Upper Stopband Attenuation.
$a[n]$, $a[k]$	filter coefficients.
D	Damper coefficient.
E	Stored energy in the FESS.
f_c	Cutoff frequency of FIR filter.
$f_{c\ max}, f_{c\ min}$	Max and min cutoff frequency of filter.
$f_{MG,N}$	Actual and Nominal frequency of MG.
$Fpass$	Passband Frequency.
$Fpass1$	Lower Passband Frequency.
$Fpass2$	Upper Passband Frequency.
Fs	Sampling Frequency.
$Fstop$	Stopband Frequency.
$Fstop1$	Lower Stopband Frequency.
$Fstop2$	Upper Stopband Frequency.
i_{1d}, i_{2d}, i_{3d}	D-axis output currents of DGE, LE and BESS.
i_{4d}, i_{sd}	D-axis output currents of G-side and M-side converters of FESS.
i_{1q}, i_{2q}, i_{3q}	Q-axis output currents of DGE, LE and BESS.
i_{4q}, i_{sq}	Q-axis output currents of G-side and M-side converters of FESS.
$i_{sq\ max}$	Maximum current along q-axis.
J	Flywheel momentum of inertia.
K	Index for the number of delays.
$k_p, k\ i$	Proportional and Integra gain.
L_s, L_r, L_m	Stator, rotor and mutual inductance.
t, n	Time.
N	Order of the filter (number of delays).
p	Number of poles of induction machine.
$P_{IM\ rat}$	Injected power of FESS.
P_{LE}, Q_{LE}	LE active and reactive power.
R_s, R_r	Stator and rotor resistancees.
T_e, T_{mech}	Electrical and mechanical torque of FESS.
T_M, Φ_M	Electrical torque and Flux of induction machine.
$V_d{}^{conv}$	Input signal of dq0 to abc converter on the daxis.
$V_q{}^{conv}$	Input signal of dq0 to abc converter on the qaxis.
v_{1d}, v_{2d}, v_{3d}	D-axis output voltages of DGE, LE and BESS.
v_{1q}, v_{2q}, v_{3q}	Q-axis output voltages of DGE, LE and BESS.
$v_{sd}, i_{sd}, \lambda_{sd}$	Voltage, current and flux of stator in d-axis.
$v_{sq}, i_{sq}, \lambda_{sq}$	Voltage, current and flux of stator in q-axis.
$v_{rd}, i_{rd}, \lambda_{rd}$	Voltage, current and flux of rotor in d-axis.
$v_{rq}, i_{rq}, \lambda_{rq}$	Voltage, current and flux of rotor in q-axis.
V_{DC}	DC link voltage.
ω_s, ω_r	Electrical angular speed of stator and rotor flux.
ω_{mech}	Mechanical speed of rotor.
ω_{IM}	Speed of induction machine.
	Measured and rated flywheel speeds.
$\omega_{max}, \omega_{min}$	Max and min of safe operation speed of FESS.
$X(n-k)$	Input to the filter at time n-k.
$Y[n]$	Output of the filter at time n.
Z^{-n}	Delay of the input at time n.

I. INTRODUCTION

Microgrids (MGs) are self-contained power systems that combine distributed generation (DG) sources, energy storage, and various power-consuming devices. They offer a host of advantages to both consumers and power system operators. Among these benefits are decreased transmission losses, enhanced power quality and reliability, and improved overall system efficiency. A control system manages MGs, allowing them to operate both independently from and connected to the main power grid [1]. For consumers, MGs provide a more reliable energy supply. By generating and storing power locally, MGs can maintain electricity availability even when the main grid experiences outages or disruptions. Power grid operators see MGs as a way to improve the efficiency and reliability of the overall power system. They help reduce transmission losses by generating electricity closer to where it is used, which means less energy is wasted during transportation. The enhanced power quality provided by MGs ensures that the electricity supplied meets higher standards, reducing the risk of damage to sensitive equipment [2]. These advantages make MGs a valuable component of modern power systems. Diesel generators are among the cost-effective DG units utilized in MGs. Usually equipped with a governor system to regulate frequency, they face a limitation arising from the extended time constant of their fuel injection system. Consequently, they are unable to have fast respond to rapid load changes leading to sudden drops in MG frequency [3], [4]. Therefore, frequency as well as voltage control in MGs are considered as a challenging task. Presently, ESSs are used to overcome these problems. These systems boast rapid response times and are integrated into MGs via power electronic converters to stabilize the grid by absorbing and injecting power as required [5], [6]. Nowadays, ESSs with high power injection capability, like supercapacitors, superconducting magnetic energy storage systems (SMESs), and FESSs, can quickly and frequently charge and discharge with high efficiency. They are suitable for enhancing stability and load levelling in power systems, managing pulse loads, and facilitating transportation [7]. Conversely, BESSs boast

high energy injection density but exhibit limited charging and discharging capabilities. By combining the features of both BESS and FESS, it becomes feasible to mitigate harsh dynamics associated with BESSs and improve battery lifespan [8]. A study by [9], have made a comparison regarding the impact of FESS and BESS over future power systems.

A two-level hierarchical strategy is proposed in [10] for energy management and control. This approach aims to reduce peak demand in electricity distribution networks by using FESS. The proposed plan creates active management in distribution networks and increases load demand growth and the hosting capacity of PV facilities. One of the critical parameters in FESS is its power and energy rating, which has an essential effect on dynamic performance in frequency control applications. Due to its quick response time and ability to handle large amounts of power, a FESS is effective in maintaining stable electricity frequency in power systems with low inertia. A new adaptive droop controller designed for a FESS is presented in [11]. This controller balances the benefits and drawbacks of the storage technology for real-world use. The new controller enhances the FESS's role in providing frequency support at the beginning of a disturbance but decreases its output as the frequency stabilizes. A nonlinear controller for FESS, utilizing model predictive control, is suggested in [12]. This method allows for managing limitations on system conditions and operations. Furthermore, the algorithm presented minimizes variations in DC link voltage and can regulate flywheel rotation speed. Due to the uncertainty in power generation of wind farms, the use of FESS in wind farms causes energy balance and frequency regulation [13], [14]. In [15], the authors developed and applied a coordinated control system for distributed BESSs. This system was designed to improve the stability and reliability of the Korean power grid by reducing fluctuations in frequency and voltage within the distribution network. A combined approach to managing solar power systems with maximum power point tracking (MPPT) and BESS is outlined in [16]. This method is intended to maintain stable voltage and frequency (V-f) levels in an isolated MG. The aim is to improve the isolated energy system's stability and dependability. In addition, the study offers recommendations for managing active and reactive power flow when connected to the main power grid. These guidelines apply to both solar panels and batteries.

The authors of study [17] utilized a hybrid energy storage system (HESS) capable of delivering high power and energy to extend battery life and boost charging capacity. To fulfil this objective, a hybrid battery configuration, comprising both high-power (HP) and high-energy (HE) battery cells, has been implemented to cater to a wider spectrum of customer requirements. The focus in [18] is on managing the energy flow between batteries and ultracapacitors within a HESS. The system uses a filter that adjusts its filtering range based on how much charge is left in the ultracapacitor. A real-time control strategy has been adopted for managing power distribution in this hybrid system. Its objectives are to safeguard the battery from damage and prolong its life, while also boosting efficiency through the power supplied by the ultracapacitor. The fundamental challenge in vehicle electrification is choosing the best ESS [19], [20]. The cost-effectiveness of fast charging stations for electric vehicles enhanced with battery-flywheel energy storage is examined in [21]. Furthermore, [22] investigates a hybrid energy system that integrates flywheels and lithium batteries to tackle efficiency reductions in lithium battery systems due to significant current fluctuations from abrupt changes in vehicle load. In [23] the authors employed a combined storage solution featuring both a lithium battery and a supercapacitor to enhance the engine's performance in a military hybrid vehicle. Likewise, the particle swarm optimization (PSO) technique is used to refine design parameters and adjust controllers. The researchers in [24] and [25] have used FESS for MG transient responses and BESS to respond to long-term load changes.

In [26] and [27], the management of frequency control in MGs involves incorporating DGs and ESSs. Each DG unit is fitted with a hierarchical control system, utilizing the droop method for primary control. Additionally, the system facilitates easy integration of DGs with plug-and-play capabilities.

The coordination between diesel generator and FESS to participate in the frequency control of a university campus MG has been investigated in [28]. Using the Finite Impulse Response (FIR) filter instead of the Butterworth filter improves the frequency drop in moments of sudden load application by the load emulator. However, in this article, to enhance frequency stability, a combination of FESS and BESS is utilized for frequency control. Additionally, using FESS along with BESS will increase the lifespan of BESS.

This study introduces a coordinated control system for both BESS and FESS to regulate the frequency of a standalone MG. In [25], the control systems for FESS and BESS are not discussed, while this study introduces precise control systems for the correct operation of FESS, BESS, DGE and LE.

Control strategies in MGs, as outlined in [29], are categorized into four main approaches: centralized control, decentralized control, distributed control, and hierarchical structure-based control. Each method offers unique advantages and challenges, depending on the specific requirements and configurations of the MG. Centralized control provides a unified decision-making process, ensuring global optimization, while decentralized control emphasizes local autonomy and flexibility. Distributed control strikes a balance between centralized and decentralized methods, promoting scalability and resilience. Finally, hierarchical control integrates multiple layers of control to achieve coordination and adaptability. These strategies collectively enhance the efficiency and reliability of MG operations. The hierarchical control system consists of three main sub-layers: primary layer, secondary layer, and tertiary layer [30]. Each of these sub-layers is assigned distinct tasks, with separate controllers employed to

execute them. A comparable structure is also adopted for the MG under investigation.

The innovation of this research lies in the development of a coordinated control strategy for HESS including FESS and BESS, to improve frequency regulation in diesel generator-based MGs. The main contributions of this research are as follows:

- Development of an advanced coordinated control approach that optimally combines the fast response capability of the FESS with the long-term energy support of the BESS. This approach reduces the pressure on the diesel generator while improving the frequency stability of the MG. Additionally, this coordinated control method helps prevent sudden and unexpected frequency fluctuations and enhances the voltage oscillations of the DC link.
- The integration of the FESS with the BESS contributes to extending the overall lifespan of the energy storage system. FESS has a higher ability to charge and discharge more frequently, so using a hybrid storage system reduces the pressure on BESS, thus extending the overall energy storage system's lifespan. This feature contributes to lowering maintenance costs and increasing the system's longevity.
- Using an FIR filter instead of a Butterworth filter for frequency control improves the system's accuracy and stability in detecting frequency changes and provides better control over frequency deviations. This feature is particularly beneficial under conditions of rapid load changes, enabling the system to respond more effectively.
- Validation is performed using a programmable load simulator to test the performance of the proposed method under dynamic load variations in real-world conditions. The simulator accurately replicates dynamic loads and evaluates the system's ability to handle various load changes, ensuring the operational feasibility of the proposed method in practical applications.

The remainder of this paper is organized as follows: Section II describes the laboratory-scaled MG. Section III details the proposed control system for coordinated frequency regulation. Section IV presents the simulation results to evaluate the effectiveness of the proposed method. Finally, Section V provides the conclusion of the study.

II. IABORATORY-SCALED MG

In this study, we introduce the MG at laboratory-scaled, and present and employ the proposed control system for frequency regulation within this MG. Fig. 1 depicts the single-line diagram (SLD) for the Autonomous MG. An Autonomous MG is a self-sufficient energy system that functions independently or partially independently from the main electrical grid. It features its own energy generation sources, which may consist of renewable options such as solar panels, wind turbines, or small hydroelectric systems, as well as conventional generators powered by diesel or natural gas. Additionally, these MGs typically incorporate energy storage solutions like batteries or flywheels. Energy storage helps to balance supply and demand within the MG, ensuring stability and reliability. One of the defining features of an autonomous MG is its ability to operate in island mode. This means that if there is a disruption or outage in the main electrical grid, the MG can continue to supply power to its local area independently. This capability is crucial for ensuring continuous power supply, especially in remote or critical locations. This model comprises five distinct components: (A) Diesel Generator Emulator (DGE), (B) Load Emulator, (C) FESS, (D) BESS and constant resistive loads. Table 1 lists the parameters of the lines that connect the MG elements.

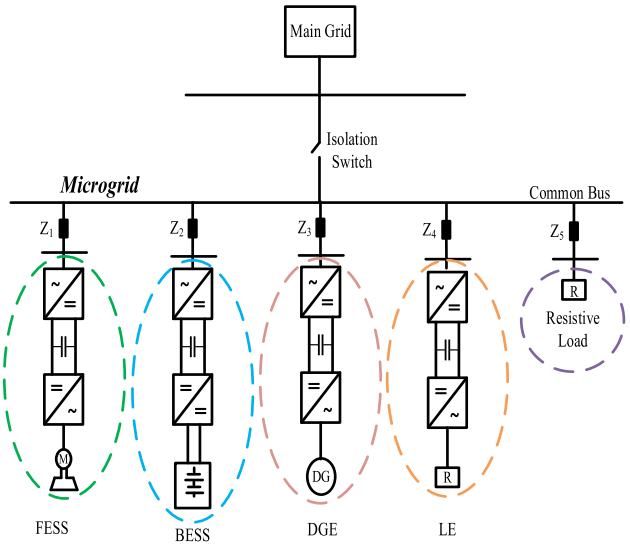

FIGURE 1. Laboratory-scaled MG schematic diagram.

A. DIESEL GENERATOR EMULATOR (DGE)

The most crucial player determining the frequency of MGs is distributed generation units based on synchronous generators such as diesel generators. The higher inertia of the diesel generator compared to other distributed generation units increases the frequency stability of an MG.

Using actual diesel generators in laboratory settings may pose certain limitations [31]. Hence, within the laboratory-scaled MG setup, a diesel generator emulator capable of replicating the performance of an actual diesel generator has been incorporated. The DGE is a controllable emulator constructed at a laboratory scale, designed utilizing power electronic converters. It is intended for stability studies and for controlling frequency and voltage in MGs. Fig. 2 shows the DGE structure used in laboratory-scaled MG. Also, Fig. 3 shows the control system used in this DGE. It includes power electronic converters (three-phase rectifier/inverter), a DC link capacitor, and LC filters [32], [33]. The input parameters of the block are calculated using Equations (1) and (2). These parameters, V_d^{conv} and V_q^{conv},

TABLE 1. Parameters of the lines connected to the MG.

Attribute	Line Resistance	Line Impedance	Line Length
FESS	0.082 Ω	500e-6 H	200 m
BESS	0.075 Ω	400e-6 H	240 m
LE	0.078 Ω	430e-6 H	50 m
DGE	0.063 Ω	520e-6 H	50 m
Resistive Load	0.056 Ω	510e-6 H	250 m

serve as the inputs to the dq0-to-abc frame transformation, respectively [34].

$$V_d^{conv} = k_p\left(i_{1d}^* - i_{1d}\right) + \int k_i\left(i_{1d}^* - i_{1d}\right) - \omega L\, i_{1q} + V_{1d} \tag{1}$$

$$V_q^{conv} = k_p\left(i_{1q}^* - i_{1q}\right) + \int k_i\left(i_{1q}^* - i_{1q}\right) + \omega L i_{1d} - V_{1q} \tag{2}$$

Information about the diesel generator under study is provided in Table 2, while Table 3 contains details about its emulator.

B. LOAD EMUULATOR (LE)

Load emulator is an effective solution to implement the behaviour of different loads in laboratory scale studies in the field of MGs. The LE models the dynamic behaviour of a load using selected equations and facilitates the study of these dynamics. It relies on power electronic converters, enabling rapid and dynamic adjustments to emulate load behaviour.

Fig. 4 shows the LE topology used in laboratory-scaled MG. Fig. 5 also shows the LE control system. The LE comprises three components: a buck converter, resistive load, and a grid-side converter functioning as a rectifier [35]. The grid-side converter is linked to the MG via an LC filter, while its DC side is connected to the buck converter through the DC link capacitor [36], [37]. The characteristics and details used in the design and implementation of this LE can be found in Table 4. The variables, i_d^* and i_q^*, are calculated by Equations (3) and (4).

$$i_d^* = \frac{3}{2}\frac{P_{LE}^*}{v_{2d}^*} \tag{3}$$

$$i_q^* = \frac{3}{2}\frac{Q_{LE}^*}{v_{2q}^*} \tag{4}$$

The input parameters of the block dq0 to abc are calculated by Equations (5) and (6).

$$V_d^{conv} = k_p\left(i_{2d}^* - i_{2d}\right) + \int k_i\left(i_{2d}^* - i_{2d}\right) - \omega L i_{2q} + V_{2d} \tag{5}$$

$$V_q^{conv} = k_p\left(i_{2q}^* - i_{2q}\right) + \int k_i\left(i_{2q}^* - i_{2q}\right) + \omega L i_{2d} + V_{2q} \tag{6}$$

TABLE 2. Selection of operating conditions and parameters for the diesel generator.

Characteristic	Value	Unit
Rating (for diesel)	3000	W
Synchronous speed (for diesel)	1500	r/min
Maximum torque (for diesel)	230	$N.m$
Inertia constant (for diesel)	2	S
Momentum of inertia (for diesel)	0.3	$Kg.m$
Rating (for generator)	3000	VA
Terminal voltage (for generator)	400	V
Number of poles (for generator)	4	-
Synchronous inertia moment (for generator)	0.1	$Kg.m2$
Synchronous speed (for generator)	1500	r/min
Frequency	50	Hz
Fuel injection time constant	35	ms
Noise level	70	db
Running time	10	s
Power factor	1	-
Colling method	Air cooled	-
Engine Type	Single cylinder	-
Chassis Enclosure	Open	-
Excitation	Self-Excited	-
Starter system	Electric start	-

TABLE 3. Selection of operating conditions and parameters for the diesel generator emulator.

Characteristic	Value	Unit
Voltage (DC Link)	700	V
Grid line voltage	400	V
Resistance of the filtering component	500	$m\Omega$
inductance of the filtering component	2	mH
capacitor of the filtering component	22	uF
Capacitor used in the DC bus system	1200	uF
Rate of switching	10	kHz
Network operating frequency	50	Hz
Droop slope	0.005	Hz/W
Droop Y-intercept	50	Hz

C. FLYWHEEL ENERGY STORAGE SYSTEM (FESS)

A FESS operates as an electromechanical device that retains energy by spinning a flywheel. Electricity is turned into rotational energy as the flywheel spins faster, and this stored energy can be changed back into electricity as the flywheel slows down. FESSs are prized for their rapid energy discharge and recharge capabilities, making them ideal for situations requiring quick power delivery or grid stabilization.

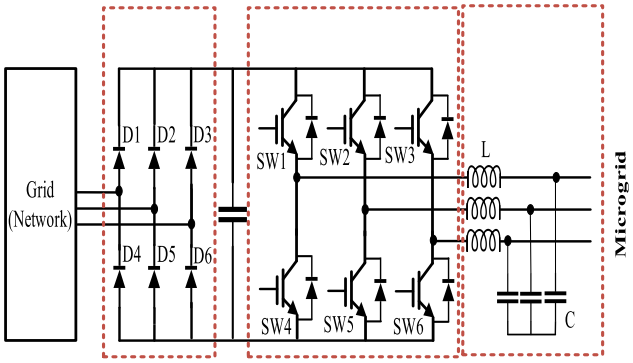

FIGURE 2. Diesel generator emulator topology.

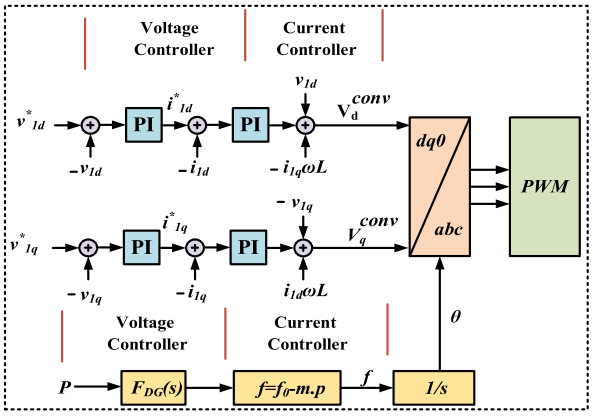

FIGURE 3. Diesel generator emulator control system.

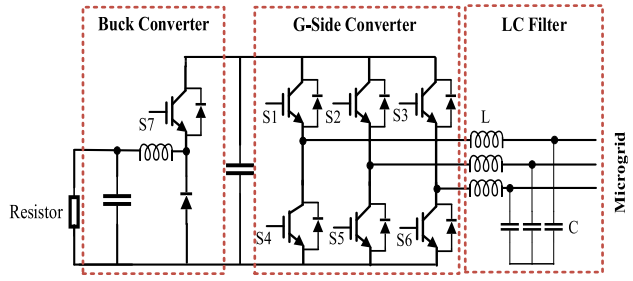

FIGURE 4. Load emulator topology.

TABLE 4. Selection of operating conditions and parameters for the load emulator.

Characteristic	Value	Unit
LE Rated power (PLE)	3000	*W*
DC-bus Voltage (VDC)	700	*V*
AC source Voltage (es)	400	*V*
Chopper output voltage range (VCH)	300	*V*
filter Resistance (R)	480	*mΩ*
filter Inductance (L)	12	*mH*
Filter capacitor	22	*uF*
AC source Inductance (L1)	2	*mH*
Leakage Inductance (L2)	2	*mH*
Buck converter switching Frequency (fs)	20	*kHz*
AC source frequency (f)	50	*Hz*
Buck converter Inductance (LB)	3	*mH*
DC link Capacitor and Buck converter output capacitor (CB)	1200	*uF*
Variable resistive load (R)	30	*mΩ*
Microcontroller type	TMS320F28 335	-

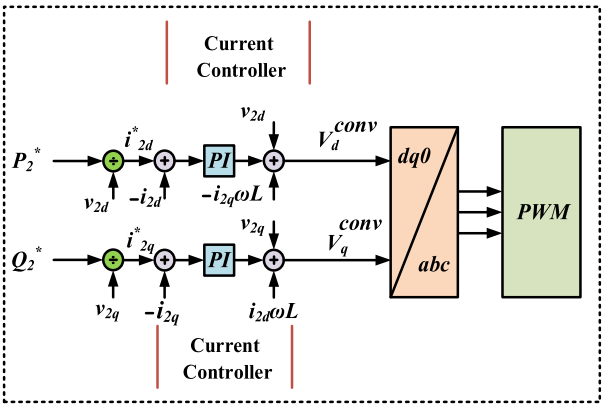

FIGURE 5. Load emulator control system.

They are highly efficient, have a long operational life, and need minimal maintenance due to the absence of chemical components. Fig. 6 illustrates the structure of the FESS used in a laboratory-scaled MG. The electric circuit comprises five main components: an inertia disc coupled with an asynchronous AC machine, a machine-side converter, a grid-side converter, an LC filter, and a DC link capacitor. This configuration ensures efficient energy conversion and storage, supporting stable MG operation. The integration of these components enables precise control and dynamic response, making the FESS a reliable solution for enhancing MG performance under various operational scenarios.

The FESS has an electric machine, and its shaft is connected to a body with a cylindrical moment of inertia called a flywheel. Two varieties of FESS exist: high-speed and low-speed. The high-speed version incorporates a disk with minimal inertia, whereas the low-speed variant utilizes a disk with substantial inertia [38], [39]. To connect the FESS to an AC MG, two power converters are needed to control the charging and discharging of the flywheel [24]. The amount of energy stored in the FESS as rotational energy is shown in Equation (7).

$$E = \frac{1}{2}J\omega^2 \tag{7}$$

In this case, ω stands for the flywheel's rotational speed, and J represents its resistance to change in rotation (moment of inertia). Equation (8) presents the mathematical formula for determining the amount of energy stored within the FESS.

$$\mathrm{D}E = \frac{1}{2}(\omega_{\max}^2 - \omega_{\min}^2) \tag{8}$$

where ω_{max} and ω_{min} represent the highest and lowest speeds of the FESS, respectively.

1) INDUCTION MACHINE MODEL

The equations concerning induction motor modeling utilized in FESS are displayed in Equations (9) and (10) [3].

$$\frac{d}{dt}\begin{bmatrix}\lambda_{sd}\\ \lambda_{sq}\end{bmatrix} = \begin{bmatrix}v_{sd}\\ v_{sq}\end{bmatrix} - R_s\begin{bmatrix}i_{sd}\\ i_{sq}\end{bmatrix} - \omega_s\begin{bmatrix}0 & -1\\ 1 & 0\end{bmatrix}\begin{bmatrix}\lambda_{sd}\\ \lambda_{sq}\end{bmatrix} \quad (9)$$

$$\frac{d}{dt}\begin{bmatrix}\lambda_{rd}\\ \lambda_{rq}\end{bmatrix} = \begin{bmatrix}v_{rd}\\ v_{rq}\end{bmatrix} - R_r\begin{bmatrix}i_{rd}\\ i_{rq}\end{bmatrix} - \omega_r\begin{bmatrix}0 & -1\\ 1 & 0\end{bmatrix}\begin{bmatrix}\lambda_{rd}\\ \lambda_{rq}\end{bmatrix} \quad (10)$$

The following equation can be used to calculate the rotor's electrical angular speed (ω_r) and the stator flux (ω_s).

$$\omega_r = \omega_s - \frac{P}{2}\omega_{mech} \quad (11)$$

In this equation, ωmech denotes the rotor's mechanical speed. The interactions between fluxes and currents are characterized by the rotor, stator, and mutual inductances (L_r, L_s, and L_m, respectively), as detailed in Equation (12).

$$\begin{bmatrix}\lambda_{sd}\\ \lambda_{sq}\\ \lambda_{rd}\\ \lambda_{rq}\end{bmatrix} = \begin{bmatrix}L_s & 0 & L_m & 0\\ 0 & L_s & 0 & L_m\\ L_m & 0 & L_s & 0\\ 0 & L_m & 0 & L_s\end{bmatrix}\begin{bmatrix}i_{sd}\\ i_{sq}\\ i_{rd}\\ i_{rq}\end{bmatrix} \quad (12)$$

The electrical torque applied to the shaft is determined as shown in Equation (13).

$$T_e = \frac{p}{2}(\lambda_{rq}i_{rd} - \lambda_{rd}i_{rq}) \quad (13)$$

In Equation (13), p is the number of poles. Finally, Newton's law is written as shown in Equation (14).

$$J\frac{d\omega_{mech}}{dt} + D\omega_{mech} = T_e - T_{mech} \quad (14)$$

where D represents the coefficient of the damper.

D. BATTERY ENERGY STORAGE SYSTEM (BESS)

A BESS captures and retains electrical energy for future use through rechargeable batteries such as lithium-ion or lead-acid. It manages energy supply and demand by storing surplus power from renewable sources or the grid and discharging it during high-demand periods. BESSs enhance grid reliability, reduce energy expenses, and enable better integration of fluctuating renewable energy sources. Its applications range from residential and commercial uses to large-scale utility operations. As seen in Fig. 7, the BESS includes a battery bank, bidirectional DC/DC converter, grid side converter, and LC filter. Lead-acid batteries are used with the energy capacity of 3.5 kWh and nominal voltage of 250 V.

III. PROPOSED CONTROL SYSTEM

The primary aim is to introduce the suggested control mechanism for incorporating the BESS into the laboratory-scaled MG, particularly to manage frequency. In the next step, the proposed method will be discussed for frequency control using FESS, and finally, a hierarchical control system is explained for frequency control of laboratory-scaled MG with the participation of FESS and BESS.

A. PROPOSED CONTROL SYSTEM FOR BESS

The BESS-generated power is delivered to the DC link by the bi-directional DC/DC converter and then transferred to the MG through the grid-side converter. The DC/DC converter is responsible for keeping the DC link voltage steady. The frequency control system for the BESS is configured along the d-axis and consists of a frequency controller and a Butterworth high-pass filter (HPF). The frequency output from the Distributed Generation Unit (DGE) is measured against the MG's reference frequency, which is established at 50 Hz. The output of the PI controller, after passing through the HPF, sets the reference current for the d-axis current (i^*_{d3}) controller. The voltage for the d-axis (v_{d3}) is created. Meanwhile, a controller adjusts the current on the q-axis (v_{q3}) to produce the corresponding voltage. The output from the current controllers is converted into a three-phase (abc) system. Subsequently, the pulse width modulation (PWM) unit produces the necessary switching signals for the grid-side converter of the BESS. Fig. 8 depicts the control system for the grid-side converter of the BESS.

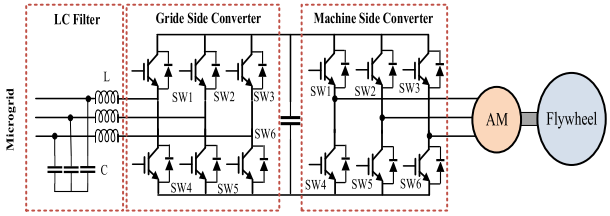

FIGURE 6. Flywheel energy storage system topology.

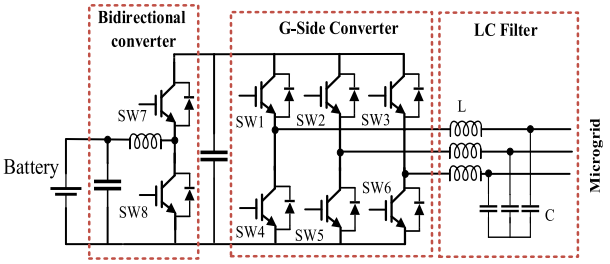

FIGURE 7. Battery energy storage system topology.

B. PROPOSED CONTROL SYSTEM FOR FESS

The FESS has two operation modes: startup mode and frequency compensation mode. In startup mode, the FESS is considered as a consumer in laboratory-scaled MG. The flywheel receives power from the MG and is charged by the electric motor up to the reference speed 3000 rpm. Once the rated speed is reached, the control mode will transition to the frequency compensation mode. We will first explore the

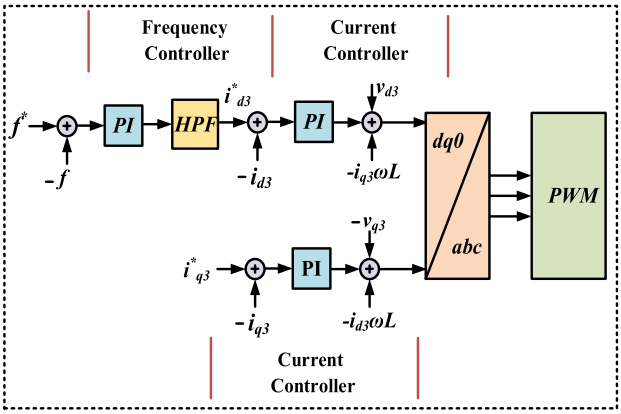

FIGURE 8. Grid side converter control system of BESS.

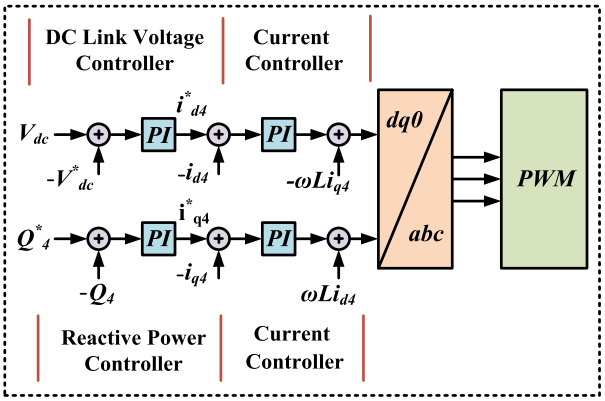

FIGURE 9. Grid side converter control system of FESS.

details of the suggested control system for the grid-side converter. Afterward, we will offer a comprehensive overview of the proposed control system for the machine-side converter.

1) GRID SIDE CONVERTER CONTROL SYSTEM

The control system for the grid-side converter employs cascaded PI controllers implemented within the dq frame. Two controllers are used on the d-axis: one to regulate the DC link voltage and another to control the electrical current flowing through the stator in the same direction. The value of i^*_{d4}, which serves as the reference for d the axis current, is derived from the DC link voltage controller's output. The desired current is compared to the actual current (i_{d4}), and the difference is used as input for the PI current controller. Within the q-axis, you'll find both the reactive power controller and the current controller (i_{q4}) (representing stator current in the q-axis). The reference current flow on the q-axis (i^*_{q4}) is determined by the output of the reactive power controller. Then, it is compared with the reactive power measured in the induction machine, serving as the input for the PI current controller. The reference voltage level (V^*_{dc}) for controlling the PWM on the d and q axes are determined by the output of the current controllers on the respective axes. The control system for the grid-side converter is shown in Fig. 9.

$$\varphi_{ref}(\omega_{IM}) = \frac{P_{IMrat} L_r}{pMi_{sq\max}\omega_{IM}} \tag{15}$$

2) MACHINE SIDE CONVERTER CONTROL SYSTEM

Fig. 10 illustrates the control system used for the machine-side converter in the FESS. Upon receiving power from the MG, the flywheel undergoes charging until it reaches its nominal speed of 3000 *rpm*. This charging process takes approximately 22 *s*. However, for simulation purposes and due to presentation constraints, an initial speed of 2800 *rpm* is assumed for the flywheel. Subsequently, it transitions into frequency compensation mode. Upon the application of a step load to the MG, the Frequency-Regulation System FESS machine-side converter for frequency control is engaged.

On the d-axis, the frequency generated by the DGE is measured against the reference frequency (f^*). It is then processed by the frequency controller. To manage the sudden injection of high power from the FESS, A Butterworth HPF is used to respond to the high frequency components in the MG power. Furthermore, low power frequency terms are compensated by the DGE. The nominal speed of the flywheel is subtracted from the output of the HPF, and this result is then supplied to the speed control layer as a reference speed. Within the speed controller, the reference speed (ω^*) undergoes comparison with the speed recorded by the encoder attached to the induction machine's shaft The induction machine is controlled using a Field Oriented Control system (FOC). The FOC in d-axis consists of torque and current controllers. The torque reference (T^*_M) is generated by the speed controller. The FOC on the q-axis includes flux and current controllers arranged in cascade. The reference flux (Φ^*_M) in the FOC method is calculated by Equation (15). In this Equation, P_{IMrat} is the power that the flywheel injects into the MG. L_r represents the rotor's inductance, M stands for the mutual inductance, i_{sqmax} indicates the maximum current along the q-axis, and ω_{IM} denotes the induction machine's speed. The stator voltages (v_{sd} and v_{sq}) produced by the present controllers in the d and q axes are transformed back to the three-phase system (abc) through reverse Park transformation. Finally, the switching pulses are sent by the PWM unit to the machine-side converter.

3) PROPOSED CONTROL STRATEGY FOR COORDINATION OF FESS AND BESS

In standalone MGs, the main-secondary control method designates the FESS with primary control duties and the BESS with secondary control functions [40]. As discussed earlier, the FESS provides substantial power density and is employed to handle power fluctuations during brief events, while the BESS, with its greater energy density, is used to manage prolonged changes in load. In this section, a hierarchical control system for HESS including FESS and BESS, for frequency control of off-grid laboratory-scaled MG,

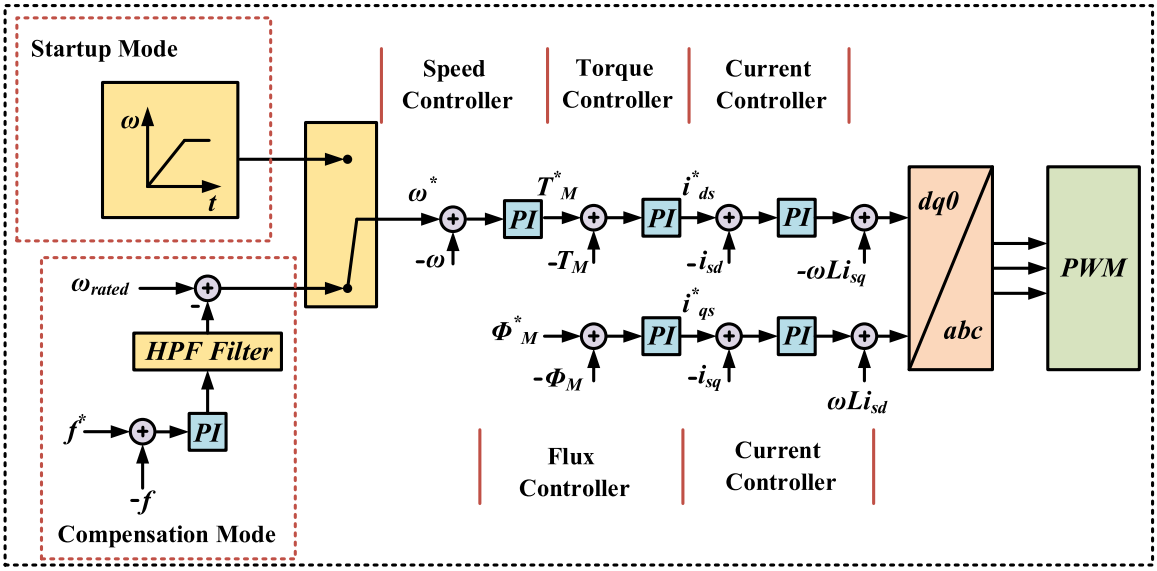

FIGURE 10. Machine side converter control system of FESS.

is presented. A new algorithm that leverages frequency distribution allocates high, medium, and low power frequencies to the FESS, BESS, and DGE, respectively, through the use of high-pass, band-pass (BPF), and low-pass (LPF) filters.

To find the best settings for the PI controllers, we created a goal based on how much and how long the frequency changes. This is explained in more detail below in Equation (16).

$$of = \int_0^t |f_{MG} - f_N| \, .tdt \tag{16}$$

where, f_{MG} is the actual frequency of the MG , f_N denotes the nominal frequency and t presents the time. The Butterworth filter, despite its widespread applications, has several notable disadvantages. These include a long-time delay, overshoot, and oscillations in the step response at certain orders, as well as reduced accuracy as the filter degree increases. These drawbacks can limit its effectiveness in scenarios requiring rapid response and high precision. Therefore, to solve the above issues, FIR filter is used instead of Butterworth filter. The specifications for the constructed HPF and BFP filters can be found in Tables 5 and 6, respectively. The control system of the DGE incorporates a LPF. According to Equation (17), the cutoff frequency of the FIR filter (f_c) is constrained between two parameters, $f_{c\,max}$ and $f_{c\,min}$. As detailed in Equation (17), the FIR filter's cutoff frequency is restricted by two values: f_c max and $f_{c\,min}$. Decreasing f_c results in increased power fluctuations compensated by both FESS and BESS. On the other hand, the maximum cutoff frequency f_c ($f_{c\,max}$) is limited by the flywheel's moment of inertia and the battery's chemical constraints. Equation (18) describes the FIR filter of causal Nth order with transfer function $A(z)$. Equation (19) describes how the FIR filter performs with respect to variations in the time domain. The transposed structure of the FIR filter is depicted in Fig. 11.

$$f_{c\,\min} \leq f_c \leq f_{c\,\max} \tag{17}$$

$$A(z) = \sum_{n=0}^{N} a\,[n] z^{-n} \tag{18}$$

$$y\,[n] = \sum_{k=0}^{N} a\,[k] x(n-k) \tag{19}$$

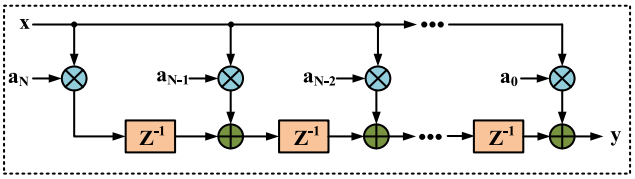

FIGURE 11. Transposed FIR filter.

TABLE 5. Parameters of the FIR HPF.

characteristic	Value (Unit)
Fs	48000 (*Hz*)
Fstop	2000 (*Hz*)
Fpass	12000 (*Hz*)
Astop	80
Apass	1

The advantages of FIR filters over Butterworth filters in frequency control and coordination between FESS, BESS,

TABLE 6. Parameters of the FIR BPF.

characteristic	Value (Unit)
Fs	48000 (*Hz*)
Fstop1	7200 (*Hz*)
Fpass1	9600 (*Hz*)
Fpass2	12000 (*Hz*)
Fstop2	14400 (*Hz*)
Astop 1	60
Apass	1
Astop1	80

and DGE are significant. First, FIR filters provide a linear and stable response because they only include coefficients based on the signal inputs. This feature is crucial in MG energy systems that require precise and undistorted responses. Additionally, unlike Butterworth filters, which require specific conditions for stability, FIR filters ensure more reliable stability under all conditions, reducing the risk of issues caused by severe frequency fluctuations. FIR filters also allow for more precise design according to the system's needs, which is especially important when managing frequency changes between FESS, BESS, and diesel generators. Furthermore, due to their precise design, FIR filters can control frequency fluctuations more effectively than Butterworth filters, particularly in situations where rapid frequency changes demand a quick response. Finally, the design and implementation of FIR filters in software like MATLAB/Simulink are simpler than with Butterworth filters, and they can be easily adapted to different systems. These advantages make FIR filters a suitable choice for improving frequency coordination and managing fluctuations in diesel generator-based MG systems using FESS and BESS.

IV. SIMULATION RESULT

In this part, we will thoroughly assess the suggested control system's effectiveness by providing simulation results for the models and systems previously examined. These results are presented across four scenarios utilizing MATLAB/SIMULINK software.

In the first scenario, the DGE and LE along with resistive loads are linked to the MG, excluding any ESS within the MG. Additionally, the LE impose a step load change on the MG. In scenario 2, the BESS is linked to the MG, incorporating DGE, LE, and resistive loads. A Butterworth HPF is used to direct high-frequency power components to the BESS. Additionally, the LE introduces a step load variation to the MG. In scenario 3, the FESS is linked to the MG, comprising the DGE, LE, and resistive loads. A Butterworth HPF is applied to direct high-frequency power components to the FESS. Additionally, the LE impose a step load change on the MG. In scenario 4, both the FESS and BESS are connected to the MG, including DGE, LE, and resistive loads. A hierarchical control system is implemented to manage the power contribution from the FESS, BESS, and DGE.

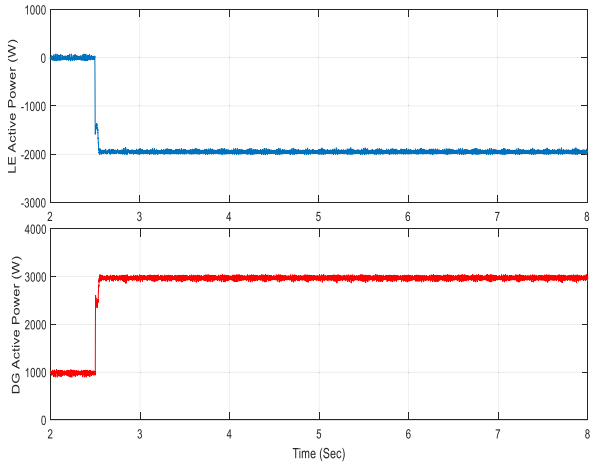

FIGURE 12. LE input power and DGE output power in first scenario.

Once more, the LE cause a step load change on the MG. Also, FIR high-pass and FIR band-pass filters are used to control the MG frequency during load changes.

A. SCENARIO 1

Initially, the resistive load uses 1000 W of active power, while the load emulator's active and reactive power settings are both zero. At $t = 2.5\ s$, a step load is applied to increase the LE's active power reference to 2000 W. As shown in Fig. 12, the DGE adjusts to changes in load through its governor system. Fig. 13 indicates that the frequency decreases to 49.02 Hz.

B. SCENARIO 2

In this scenario, the first scenario is augmented with the inclusion of the BESS, which operates under the specified control system employing a Butterworth high-pass filter. Initially, the load emulator's active and reactive power references are adjusted to zero. At $t = 2.5\ s$, the LE's active power reference is changed to 2000 W. As shown in Fig. 14, the BESS responds to high-frequency power demands within 7.8 s due to its faster power injection rate compared to the DGE, leading to its output power falling to zero. Afterwards, the DGE smoothly adjusts to the low-frequency requirements of the power needed. As depicted in Fig. 15, the frequency decreases to 49.65 Hz. The coordination of the BESS with DGE causes less frequency drop when a sudden load is applied to the MG compared to scenario 1. Fig. 16 shows the BESS DC link voltage variation curve. At $t = 2.5\ s$, due to load changes, the DC link voltage decreases to 682.55 V and returns to the reference voltage (700 V) in a short time period. Fig. 17 illustrates the voltage and current waveform delivered by the BESS to the MG in the time interval of 2 s to 2.35 s.

C. SCENARIO 3

In the third scenario, the inclusion of the FESS into scenario 1 entails its operation based on the control system

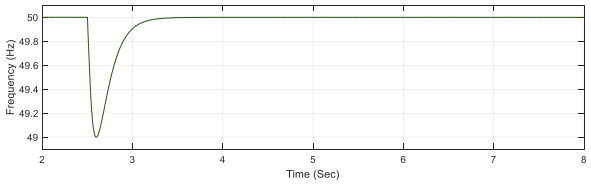

FIGURE 13. Changes in frequency during first scenario.

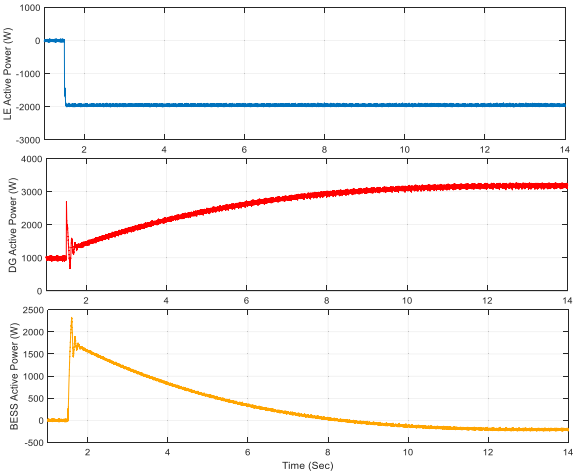

FIGURE 14. LE input power and DGE and BESS output power in second scenario.

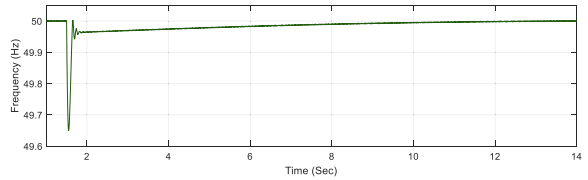

FIGURE 15. Changes in frequency during second scenario.

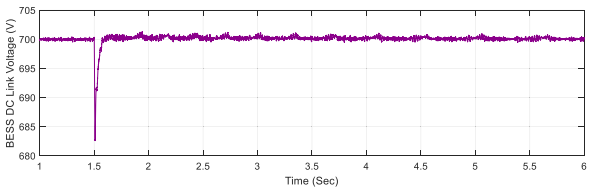

FIGURE 16. DC-link voltage changes caused by sudden load variations in second scenario.

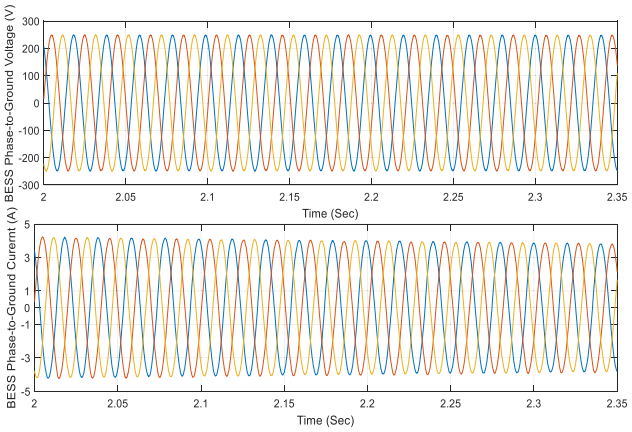

FIGURE 17. Voltage and current waveforms of the BESS resulting from a sudden load change in second scenario.

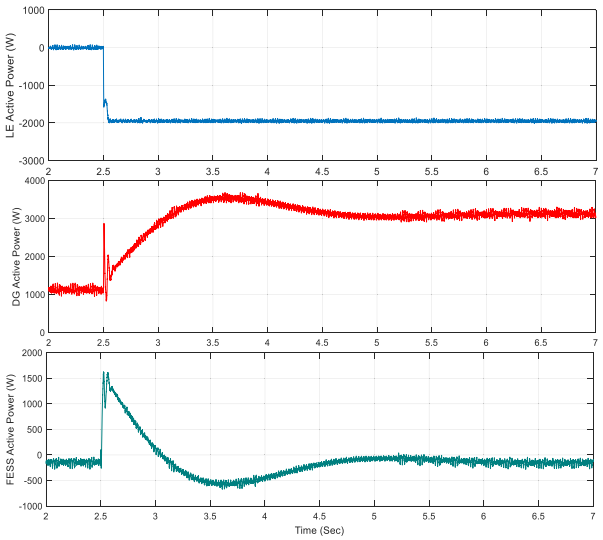

FIGURE 18. LE input power and DGE and FESS output power in third scenario.

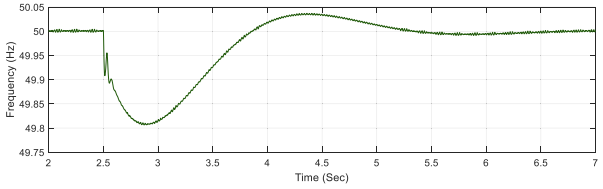

FIGURE 19. Changes in frequency during third scenario.

employing a Butterworth high pass filter Initially, the load emulator's active and reactive power setpoints are configured to zero. The active power setting for the LE is switched to 2000 W at time equals $t = 2.5\ s$. As depicted in Fig. 18, the FESS rapidly reacts to high-frequency power requirements, achieving zero output power within 2.7 s. Subsequently, the DGE adjusts seamlessly to the lower frequency components of the needed power. Fig. 19 illustrates a frequency reduction to 49.81 Hz. The collaboration between the FESS and DGE leads to a smaller frequency decrease under sudden load conditions in the MG, as opposed to what is observed in scenario 1. The fluctuations in the DC link voltage are illustrated in Fig. 20. The machine-side converter sends electrical power to the DC link, which then forwards it to the grid-side converter. Power injection in the DC link causes transient over-voltages. The DC link voltage controller, situated in the grid-side converter, maintains the DC link voltage at a steady 700 V. The maximum allowed fluctuation in the DC link voltage is 11.36 V. Fig. 21 shows the current and voltage of the three phases of the FESS output in the time interval of 2.65 s to 3 s.

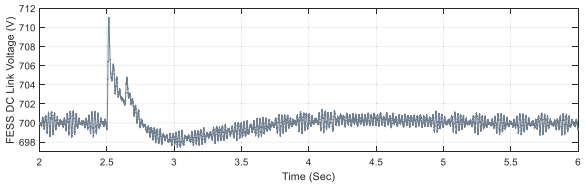

FIGURE 20. DC-link voltage changes caused by sudden load variations in third scenario.

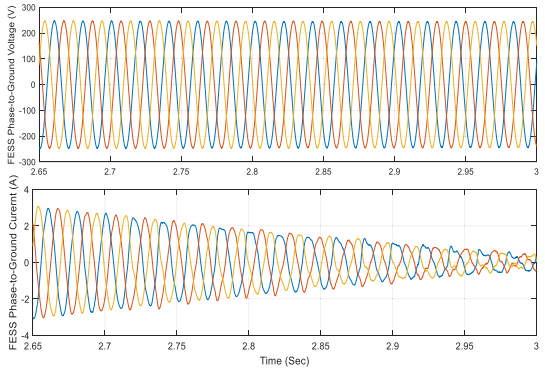

FIGURE 21. Voltage and current waveforms of the FESS resulting from a sudden load change in third scenario.

D. SCENARIO 4

In this scenario, FESS and BESS are added to the MG including, DGE, LE, and resistive loads (scenario 1). Initially, the LE's settings for active and reactive power are set to zero, and the MG only provides power to resistive loads. The desired active power output of the LE is adjusted to 2000 W at $t = 2.5\ s$, as depicted in Fig. 22. Since the BESS is an electrochemical storage, it takes some time to reach its peak power; on the other hand, the FESS can inject high power in this short time period. In fact, in this hierarchical control system, the FESS compensates for the initial fluctuations of the required power. The BESS is used in secondary control level. When the FESS and BESS deliver power for high and medium-frequency needs and are in discharge mode, the DGE takes over by supplying the low-frequency power requirements and handling the tertiary control functions. Fig. 23 illustrates that the joint contribution of FESS and BESS to the MG's frequency regulation causes the MG's frequency to decrease to 49.961 Hz. Fig. 24 shows that the changes in DC link voltage for both the BESS and FESS confirm that the proposed control system operates correctly when a load is introduced to the MG. Fig.s 25 and 26 show the curve of voltage and current injected by BESS and FESS to MG, respectively, at the moment of step load application.

E. MG PERFORMANCE UIDER PLUG-AND-PLAY CONDITIONS

Fig. 27 shows the MG performance curve under plug-and-play conditions. At $t = 1\ s$, BESS is connected to the MG but does not inject power. At $t = 2.5\ s$, an active load (2000 W) is applied to the MG, and FESS, BESS, and DGE participate

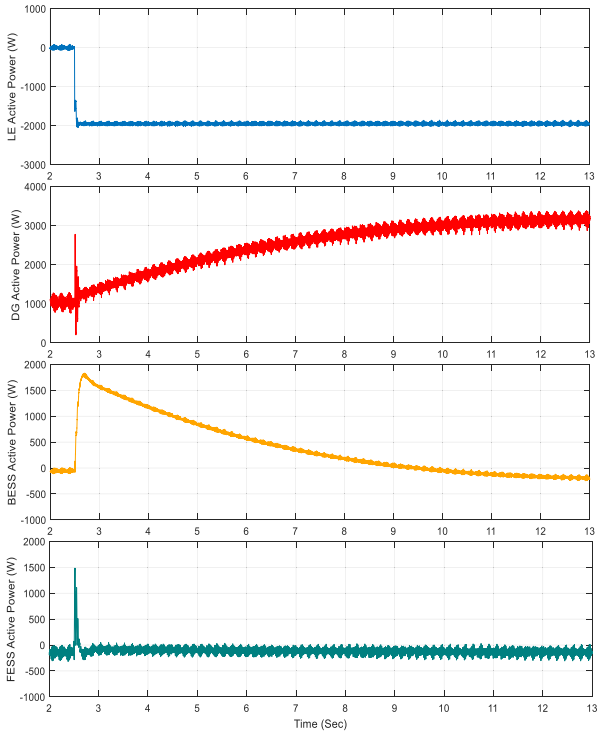

FIGURE 22. LE input power and DGE, BESS and FESS output power in fourth scenario.

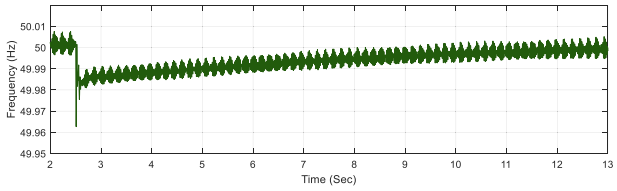

FIGURE 23. Changes in frequency during fourth scenario.

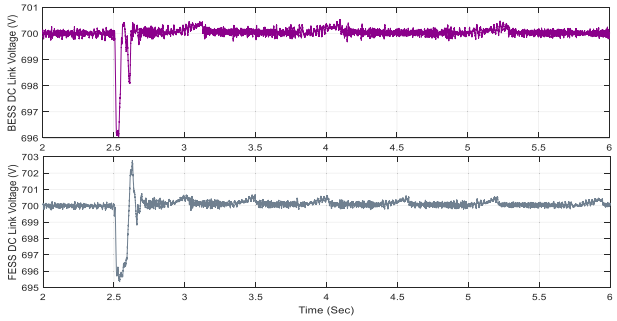

FIGURE 24. DC-link voltage changes caused by sudden load variations in fourth scenario.

in frequency control. At $t = 4\ s$, the BESS is disconnected, and its output power becomes zero, leading to a decrease in MG frequency. At $t = 5\ s$, the FESS is disconnected, causing an increase in MG frequency as the FESS enters startup mode. The transient response of the MG during these events demonstrates the dynamic interactions between the energy storage units and the diesel generator. The impact of

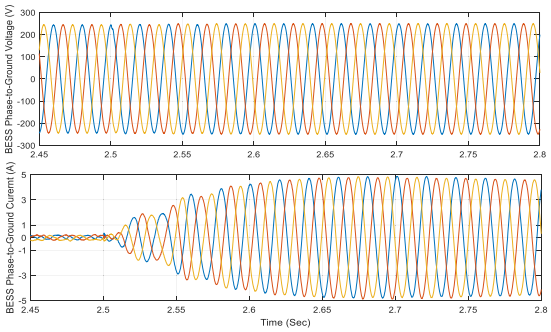

FIGURE 25. Voltage and current waveforms of the BESS resulting from a sudden load change in fourth scenario.

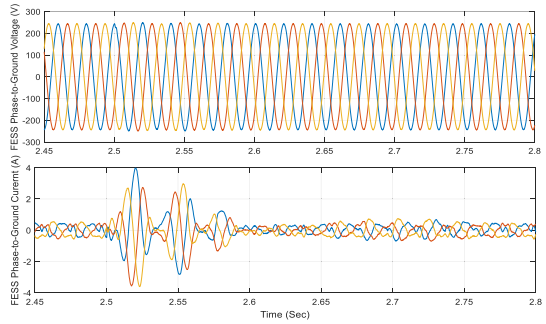

FIGURE 26. Voltage and current waveforms of the FESS resulting from a sudden load change in fourth scenario.

each component's disconnection on the frequency deviation highlights the need for coordinated control strategies. Fig. 28 shows that the frequency eventually stabilizes at its nominal value of 50 *Hz*, confirming the effectiveness of the proposed control approach. These results emphasize the importance of seamless energy storage integration to ensure stable and reliable MG operation.

F. COMPARISON OF THD IN DIFFERENT SCENARIOS OF MG FREQUENCY CONTROL

In this section of the paper, the impact of coordinated control of BESS and FESS energy storage systems on reducing total harmonic distortion (THD) in MGs is examined. Harmonic distortion is a major challenge in electrical systems, as it can damage equipment and reduce power quality. According to IEEE 519 standard, the allowable level of THD in electrical systems must be less than 3% [41]. In this study, the THD levels in four different scenarios are simulated, and the results are presented in Table 7. The different scenarios include various combinations of diesel generators, load emulators, BESS, FESS, and resistive loads for MG frequency control. The simulation results indicate that the BESS and FESS energy storage systems, especially when combined, are capable of maintaining THD levels below 3%, in accordance with IEEE 519 standards. This performance is particularly effective under dynamic load conditions and rapid load variations, demonstrating the proposed control method's effectiveness in improving power quality and MG stability. In the control

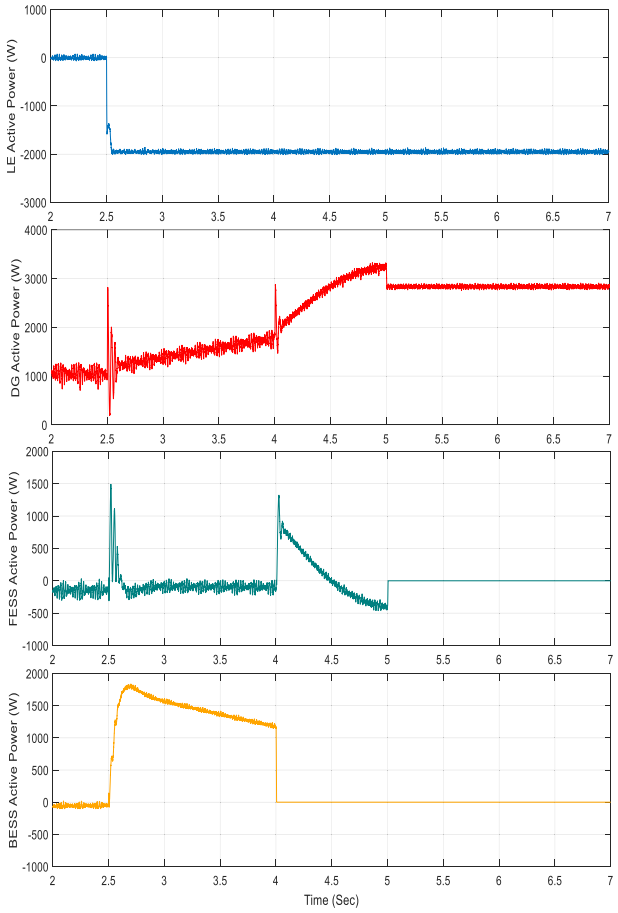

FIGURE 27. LE input power and DGE, BESS and FESS output power in plug-and-play study case.

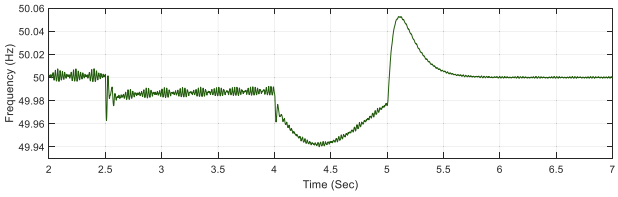

FIGURE 28. Changes in frequency during plug-and-play study case.

system of the MG converters, the THD level is set to be below 3% [42], [43].

G. COMPARISON BETWEEN FOUR SCENARIOS

Table 7 presents the frequency drop of the MG and the maximum DC link voltage deviation across four studied scenarios. In Scenario 1, the DGE alone is responsible for frequency control, and no ESS is used. As a result, the frequency drop during the application of a sudden load is 0.98 *Hz*. To improve frequency drop and oscillations, Scenario 2 utilizes a BESS. With the integration of this ESS, the frequency drop is reduced to 0.35 *Hz*, indicating the positive impact of using an ESS. In Scenario 3, due to the higher power injection speed of the FESS compared to BESS, the frequency drop is

TABLE 7. Comparison among 4 scenarios.

Scenarios	Maximum Frequency Drop	Maximum DC link Voltage Variation	THD
Scenario1	0.98 *Hz*	-	1.56%
Scenario 2	0.35 *Hz*	17.45 *V*	2.34%
Scenario 3	0.19 *Hz*	11.36 *V*	2.54%
Scenario 4	0.039 *Hz*	3.87 V | 5.43 *V*	2.68%

further reduced to 0.19 *Hz*, demonstrating the effectiveness of FESS in frequency control compared to BESS. In Scenario 4, to reduce frequency oscillations and also enhance the lifespan of ESSs, a HESS consisting of both BESS and FESS is used simultaneously. As a result, the frequency drop is minimized to 0.039 *Hz*. As observed in the final scenario, the combined use of FESS and BESS for frequency control improves the frequency drop compared to Scenarios 1, 2, and 3 by 96.02%, 88.86%, and 79.47%, respectively.

H. COMPARISON WITH OTHER REFERENCES

A coordination between a diesel generator and a FESS for frequency control in a MG is presented in [28], where a FIR filter is utilized for frequency regulation within the system. The advantage of this study lies in the proposal of a hybrid energy storage system, where frequency coordination among FESS, BESS, and DGE is implemented to improve frequency and voltage fluctuations. In [44], a frequency control system is used to mitigate fluctuations in a MG consisting of FESS, DGE, and LE. This paper employs Butterworth filters of varying orders to establish frequency coordination between FESS and DGE. The use of FIR filters in the studied paper leads to better frequency and voltage stability compared to [44]. Moreover, the application of HESS contributes to extending the lifespan of the energy storage system. In [45], a FESS system combined with fuzzy PI controllers is employed to improve frequency fluctuations in a diesel generator-based MG. Due to the absence of filters for frequency coordination between FESS and the diesel generator, frequency fluctuations are higher, a gap addressed in the current study. To enhance the reliability of the energy storage system compared to [46], a hybrid energy storage system is used in the current study, resulting in better voltage and frequency regulation. Another advantage is the use of FIR filters to establish a coordinated frequency control system among FESS, BESS, and DGE.

Table 8 shows that the proposed method outperforms other approaches in maintaining both frequency stability and DC link voltage consistency, based on maximum deviation metrics. The enhanced DC link voltage performance is primarily attributed to the implementation of an FIR filter in the control strategy. Owing to its linear phase response and precise time-domain characteristics, the FIR filter enables more accurate detection of voltage fluctuations and supports faster corrective actions.

TABLE 8. Comparison with other references.

Scenarios	Maximum Frequency Drop	Maximum DC link Voltage Variation
[44]	0.38 *Hz*	22 *V*
[28]	0.21 *Hz*	13 *V*
[45]	0.18 *Hz*	60 *V*
[46]	0.12 *Hz*	11 *V*
Proposed	0.039 *Hz*	3.87 *V* | 5.43 *V*

Consequently, DC link voltage oscillations during transient events are more effectively damped, resulting in improved overall stability and reliability of the MG.

V. CONCLUSION

In this research, an analysis of the control system for frequency coordination among the FESS, BESS, and DGE was provided. Furthermore, a comprehensive examination of the structural components and control systems employed in the DGE, LE, FESS, and BESS was conducted. The combination of FESS and BESS technologies yielded a hybrid system that excels at handling rapidly changing energy consumption patterns. The power needs of the MG were divided into different frequency ranges. A control system then assigned the high, medium, and low frequency portions to the FESS, BESS, and DGE, respectively. Due to high power injection speed, primary control was performed by FESS. This property serves as the main contributing factor to the absence of frequency drop during the initial moments of load application. Due to its high energy injection capability, the BESS undertakes secondary control, and subsequently, the diesel generator, characterized by the slower fuel injection system, implements tertiary control. It was also discussed that using FIR filter instead of Butterworth filter will improve frequency fluctuations. Besides, using this method will reduce DC link voltage fluctuations. The voltage and current harmonics stayed very low, as the control system in the converters maintained a Total Harmonic Distortion (THD) below 3%.

In this study, several limitations may affect the accuracy and applicability of the results:

- Use of Diesel Generator Emulator: Due to laboratory constraints, an emulator was used in place of a real diesel generator, which may have introduced differences in system behavior.
- Environmental and Operational Conditions: The study does not consider the impact of environmental factors like temperature and humidity, or operational system limitations.
- Long-term Effects and Equipment Degradation: The paper does not address long-term effects such as battery degradation and flywheel wear, which could affect performance over time.

At the continuation of this research, several approaches are proposed to expand and advance the studies on the use of ESSs for improving the stability of microgrids. These suggestions can contribute to the development and optimization of the performance of these systems and play a significant role in enhancing the quality and efficiency of microgrids:

- Implementation of Predictive and Robust Control Systems for FESS and BESS to Enhance MG Resilience to Disturbances
- Technical-Economic Studies for Optimizing the Sizing of FESS and BESS
- Exploring Alternative Energy Storage Systems, such as Superconductors, and Combining Them with FESS and BESS
- Expanding the Microgrid and Incorporating More Distributed Energy Resources (DERs) and Dynamic and Static Loads

REFERENCES

[1] M. Furqan and H. Boudet, "Nuances of valuing resilience from microgrids," *Renew. Sustain. Energy Rev.*, vol. 210, Mar. 2025, Art. no. 115236, doi: 10.1016/j.rser.2024.115236.

[2] S. Ahmad, M. Shafiullah, C. B. Ahmed, and M. Alowaifeer, "A review of microgrid energy management and control strategies," *IEEE Access*, vol. 11, pp. 21729–21757, 2023, doi: 10.1109/ACCESS.2023.3248511.

[3] Y. Mi, B. Chen, P. Cai, X. He, R. Liu, and X. Yang, "Frequency control of a wind-diesel system based on hybrid energy storage," *Prot. Control Mod. Power Syst.*, vol. 7, pp. 1–13, Jul. 2022, doi: 10.1186/s41601-022-00250-1.

[4] F. Hong, K. Wei, W. Ji, J. Hao, F. Fang, and J. Liu, "A cross-entropy-based synergy method for capacity configuration and SOC management of flywheel energy storage in primary frequency regulation," *Energy*, vol. 316, Feb. 2025, Art. no. 134498, doi: 10.1016/j.energy.2025.134498.

[5] S. Ali, Z. Zheng, M. Aillerie, J.-P. Sawicki, M.-C. Péra, and D. Hissel, "A review of DC microgrid energy management systems dedicated to residential applications," *Energies*, vol. 14, no. 14, p. 4308, Jul. 2021, doi: 10.3390/en14144308.

[6] S. Choudhury, "Review of energy storage system technologies integration to microgrid: Types, control strategies, issues, and future prospects," *J. Energy Storage*, vol. 48, Apr. 2022, Art. no. 103966, doi: 10.1016/j.est.2022.103966.

[7] M. Farhadi and O. Mohammed, "Energy storage technologies for high-power applications," *IEEE Trans. Ind. Appl.*, vol. 52, no. 3, pp. 1953–1961, May 2016, doi: 10.1109/TIA.2015.2511096.

[8] A. Mehraban, E. Farjah, T. Ghanbari, and L. Garbuio, "Integrated optimal energy management and sizing of hybrid battery/flywheel energy storage for electric vehicles," *IEEE Trans. Ind. Informat.*, vol. 19, no. 11, pp. 10967–10976, Nov. 2023, doi: 10.1109/TII.2023.3242580.

[9] F. Nadeem, S. M. S. Hussain, P. K. Tiwari, A. K. Goswami, and T. S. Ustun, "Comparative review of energy storage systems, their roles, and impacts on future power systems," *IEEE Access*, vol. 7, pp. 4555–4585, 2019, doi: 10.1109/ACCESS.2018.2888497.

[10] L. Tziovani, L. Hadjidemetriou, C. Charalampous, M. Tziakouri, S. Timotheou, and E. Kyriakides, "Energy management and control of a flywheel storage system for peak shaving applications," *IEEE Trans. Smart Grid*, vol. 12, no. 5, pp. 4195–4207, Sep. 2021, doi: 10.1109/TSG.2021.3084814.

[11] S. Karrari, G. De Carne, and M. Noe, "Adaptive droop control strategy for flywheel energy storage systems: A power hardware-in-the-loop validation," *Electr. Power Syst. Res.*, vol. 212, Nov. 2022, Art. no. 108300, doi: 10.1016/j.epsr.2022.108300.

[12] M. Ghanaatian and S. Lotfifard, "Control of flywheel energy storage systems in the presence of uncertainties," *IEEE Trans. Sustain. Energy*, vol. 10, no. 1, pp. 36–45, Jan. 2019, doi: 10.1109/TSTE.2018.2822281.

[13] A. A. Thatte, F. Zhang, and L. Xie, "Coordination of wind farms and flywheels for energy balancing and frequency regulation," in *Proc. IEEE Power Energy Soc. Gen. Meet.*, Jun. 2011, pp. 1–7, doi: 10.1109/PES.2011.6039118.

[14] J. Yao, M. Yu, W. Gao, and X. Zeng, "Frequency regulation control strategy for PMSG wind-power generation system with flywheel energy storage unit," *IET Renew. Power Gener.*, vol. 11, no. 8, pp. 1082–1093, Jun. 2017, doi: 10.1049/iet-rpg.2016.0047.

[15] S.-J. Lee, J.-H. Kim, C.-H. Kim, S.-K. Kim, E.-S. Kim, D.-U. Kim, K. K. Mehmood, and S. U. Khan, "Coordinated control algorithm for distributed battery energy storage systems for mitigating voltage and frequency deviations," *IEEE Trans. Smart Grid*, vol. 7, no. 3, pp. 1713–1722, May 2016, doi: 10.1109/TSG.2015.2429919.

[16] S. Adhikari and F. Li, "Coordinated V-f and P-Q control of solar photovoltaic generators with MPPT and battery storage in microgrids," *IEEE Trans. Smart Grid*, vol. 5, no. 3, pp. 1270–1281, May 2014, doi: 10.1109/TSG.2014.2301157.

[17] F. Naseri, C. Barbu, and T. Sarikurt, "Optimal sizing of hybrid high-energy/high-power battery energy storage systems to improve battery cycle life and charging power in electric vehicle applications," *J. Energy Storage*, vol. 55, Nov. 2022, Art. no. 105768, doi: 10.1016/j.est.2022.105768.

[18] E. M. Asensio, G. A. Magallán, C. H. D. Angelo, and F. M. Serra, "Energy management on battery/ultracapacitor hybrid energy storage system based on adjustable bandwidth filter and sliding-mode control," *J. Energy Storage*, vol. 30, Aug. 2020, Art. no. 101569, doi: 10.1016/j.est.2020.101569.

[19] H. H. Eldeeb, A. T. Elsayed, C. R. Lashway, and O. Mohammed, "Hybrid energy storage sizing and power splitting optimization for plug-in electric vehicles," *IEEE Trans. Ind. Appl.*, vol. 55, no. 3, pp. 2252–2262, May 2019, doi: 10.1109/TIA.2019.2898839.

[20] J. Shen, S. Dusmez, and A. Khaligh, "Optimization of sizing and battery cycle life in battery/ultracapacitor hybrid energy storage systems for electric vehicle applications," *IEEE Trans. Ind. Informat.*, vol. 10, no. 4, pp. 2112–2121, Nov. 2014, doi: 10.1109/TII.2014.2334233.

[21] P. Mouratidis, "Augmenting electric vehicle fast charging stations with battery-flywheel energy storage," *J. Energy Storage*, vol. 97, Sep. 2024, Art. no. 112957, doi: 10.1016/j.est.2024.112957.

[22] B. Sun, M. Xie, B. Li, P. Wang, and S. Gao, "Design and application of flywheel-lithium battery composite energy system for electric vehicles," *Int. J. Automot. Technol.*, vol. 25, no. 1, pp. 107–117, Feb. 2024, doi: 10.1007/s12239-024-00017-7.

[23] A.-A. Mamun, Z. Liu, D. M. Rizzo, and S. Onori, "An integrated design and control optimization framework for hybrid military vehicle using lithium-ion battery and supercapacitor as energy storage devices," *IEEE Trans. Transport. Electrific.*, vol. 5, no. 1, pp. 239–251, Mar. 2019, doi: 10.1109/TTE.2018.2869038.

[24] T.-T. Nguyen, H.-J. Yoo, and H.-M. Kim, "A flywheel energy storage system based on a doubly fed induction machine and battery for microgrid control," *Energies*, vol. 8, no. 6, pp. 5074–5089, Jun. 2015, doi: 10.3390/en8065074.

[25] L. Shen, Q. Cheng, Y. Cheng, L. Wei, and Y. Wang, "Hierarchical control of DC micro-grid for photovoltaic EV charging station based on flywheel and battery energy storage system," *Electr. Power Syst. Res.*, vol. 179, Feb. 2020, Art. no. 106079, doi: 10.1016/j.epsr.2019.106079.

[26] S. Ullah, L. Khan, M. Jamil, M. Jafar, S. Mumtaz, and S. Ahmad, "A finite-time robust distributed cooperative secondary control protocol for droop-based islanded AC microgrids," *Energies*, vol. 14, no. 10, p. 2936, May 2021, doi: 10.3390/en14102936.

[27] S. Ullah, L. Khan, I. Sami, G. Hafeez, and F. R. Albogamy, "A distributed hierarchical control framework for economic dispatch and frequency regulation of autonomous AC microgrids," *Energies*, vol. 14, p. 8408, 2021. [Online]. Available: https://doi.org/10.3390/en14248408

[28] M. Faraji, M. S. Mahdavi, G. B. Gharehpetian, R. Ahmadiahangar, and A. Rosin, "Cooperative control of flywheel energy storage system and diesel generator for frequency regulation of microgrids using digital FIR filters," in *Proc. IEEE 17th Int. Conf. Compat., Power Electron. Power Eng. (CPE-POWERENG)*, Jun. 2023, pp. 1–6, doi: 10.1109/CPE-POWERENG58103.2023.10227448.

[29] N. Salehi, H. Martínez-García, G. Velasco-Quesada, and J. M. Guerrero, "A comprehensive review of control strategies and optimization methods for individual and community microgrids," *IEEE Access*, vol. 10, pp. 15935–15955, 2022, doi: 10.1109/ACCESS.2022.3142810.

[30] A. Tahir, J. M. Böling, M.-H. Haghbayan, and J. Plosila, "Comparison of linear and nonlinear methods for distributed control of a hierarchical formation of UAVs," *IEEE Access*, vol. 8, pp. 95667–95680, 2020, doi: 10.1109/ACCESS.2020.2988773.

[31] S. German-Galkin, D. Tarnapowicz, Z. Matuszak, and M. Jaskiewicz, "Optimization to limit the effects of underloaded generator sets in standalone hybrid ship grids," *Energies*, vol. 13, no. 3, p. 708, Feb. 2020, doi: 10.3390/en13030708.

[32] Q. Long, H. Yu, F. Xie, N. Lu, and D. Lubkeman, "Diesel generator model parameterization for microgrid simulation using hybrid box-constrained Levenberg–Marquardt algorithm," *IEEE Trans. Smart Grid*, vol. 12, no. 2, pp. 943–952, Mar. 2021, doi: 10.1109/TSG.2020.3026617.

[33] A. Ul Haq, I. Ahsan, and H. Jamil, "Virtual inertia emulation in a hybrid micro grid based on diesel generator and wind power plant," *Int. J. Eng. Works*, vol. 8, no. 1, pp. 14–17, Jan. 2020, doi: 10.34259/ijew.21.8011417.

[34] R. D. Kordkandi, M. T. Hagh, S. Roozbehani, M. Feyzi, N. Bayati, and T. Ebel, "Reactive power control of micro-grids using FOSMC for grid code compliance during asymmetrical voltage sags," *Electric Power Syst. Res.*, vol. 229, Apr. 2024, Art. no. 110056, doi: 10.1016/j.epsr.2023.110056.

[35] Z. Geng, D. Gu, T. Hong, and D. Czarkowski, "Programmable electronic AC load based on a hybrid multilevel voltage source inverter," *IEEE Trans. Ind. Appl.*, vol. 54, no. 5, pp. 5512–5522, Sep. 2018, doi: 10.1109/TIA.2018.2818059.

[36] M. Ashourianjozdani, L. A. C. Lopes, and P. Pillay, "Power electronic converter based PMSG emulator: A testbed for renewable energy experiments," *IEEE Trans. Ind. Appl.*, vol. 54, no. 4, pp. 3626–3636, Jul. 2018, doi: 10.1109/TIA.2018.2819618.

[37] H. Y. Kanaan, M. Caron, and K. Al-Haddad, "Design and implementation of a two-stage grid-connected high efficiency power load emulator," *IEEE Trans. Power Electron.*, vol. 29, no. 8, pp. 3997–4006, Aug. 2014, doi: 10.1109/TPEL.2013.2295023.

[38] A. Saleh, A. Awad, and W. Ghanem, "Modeling, control, and simulation of a new topology of flywheel energy storage systems in microgrids," *IEEE Access*, vol. 7, pp. 160363–160376, 2019, doi: 10.1109/ACCESS.2019.2951029.

[39] X. Li, B. Anvari, A. Palazzolo, Z. Wang, and H. Toliyat, "A utility-scale flywheel energy storage system with a shaftless, hubless, high-strength steel rotor," *IEEE Trans. Ind. Electron.*, vol. 65, no. 8, pp. 6667–6675, Aug. 2018, doi: 10.1109/TIE.2017.2772205.

[40] S. D. Sessa, A. Tortella, M. Andriollo, and R. Benato, "Li-ion battery-flywheel hybrid storage system: Countering battery aging during a grid frequency regulation service," *Appl. Sci.*, vol. 8, no. 11, p. 2330, Nov. 2018, doi: 10.3390/app8112330.

[41] *IEEE Recommended Practice and Requirements for Harmonic Control in Electric Power Systems*, IEEE Standard 519-2014 (Revision of IEEE Std 519-1992), pp. 1–29, Jun. 2014, doi: 10.1109/IEEESTD.2014.6826459.

[42] A. Arranz-Gimon, A. Zorita-Lamadrid, D. Morinigo-Sotelo, and O. Duque-Perez, "A review of total harmonic distortion factors for the measurement of harmonic and interharmonic pollution in modern power systems," *Energies*, vol. 14, no. 20, p. 6467, Oct. 2021, doi: 10.3390/en14206467.

[43] B. Indu Rani, G. Saravana Ilango, and C. Nagamani, "Control strategy for power flow management in a PV system supplying DC loads," *IEEE Trans. Ind. Electron.*, vol. 60, no. 8, pp. 3185–3194, Aug. 2013.

[44] M. S. Mahdavi, M. Bagheri, and G. B. Gharehpetian, "Coordinated frequency control of flywheel energy storage and diesel generator in amirkabir university of technology (AUT) microgrid," in *Proc. IEEE Int. Conf. Environ. Electr. Eng. IEEE Ind. Commercial Power Syst. Eur. (EEEIC/ICPS Eur.)*, Jun. 2019, pp. 1–6, doi: 10.1109/EEEIC.2019.8783670.

[45] M. S. Mahdavi, G. B. Gharehpetian, P. Ranjbaran, and H. Azizi, "Frequency regulation of AUT microgrid using modified fuzzy PI controller for flywheel energy storage system," in *Proc. 9th Annu. Power Electron., Drives Syst. Technol. Conf. (PEDSTC)*, Feb. 2018, pp. 426–431, doi: 10.1109/PEDSTC.2018.8343835.

[46] M. S. Mahdavi, G. B. Gharehpetian, and H. A. Moghaddam, "Enhanced frequency control method for microgrid-connected flywheel energy storage system," *IEEE Syst. J.*, vol. 15, no. 3, pp. 4503–4513, Sep. 2021, doi: 10.1109/JSYST.2020.3010029.

MAHDI FARAJI was born in Markazi, Iran, in May 1998. He received the B.Sc. degree in electrical engineering and the M.Sc. degree in power systems engineering from the Amirkabir University of Technology (AUT), Tehran, Iran, in 2020 and 2023, respectively. During his master's studies, he contributed significantly to the design and implementation of the laboratory microgrid with AUT, focusing on frequency control and the integration of distributed generation and energy storage systems. His research interests include microgrids, renewable energy systems, distributed generation, and energy storage systems, with a particular emphasis on enhancing grid stability and reliability.

MOHAMMAD SAEED MAHDAVI received the B.Sc. degree in power engineering from Isfahan University of Technology, Isfahan, Iran, in 2012, and the M.Sc. and Ph.D. degrees in power engineering from the Amirkabir University of Technology (AUT), Tehran, Iran, in 2014 and 2019, respectively.

He is currently an Assistant Professor with the Electrical and Computer Engineering Department, Isfahan University of Technology. From 2014 to 2022, he was the Technical Manager of AUT Microgrid project as one of the sub-projects of Iran Grand (National) Smart Grid Project under the supervision of Prof. G. B. Gharehpetian. His current research interests include power electronics, microgrids, electric drives, energy storage systems, DGs, and electric vehicles.

Dr. Mahdavi was a recipient of three national prizes, as the Best Dissertation Award from Power Electronics Society of Iran, in February 2020, Iranian Scientific Organization of Smart Grids, in 2020, and AUT for his Ph.D. dissertation, in 2020.

VENERA NURMANOVA was born in Zhezkazgan, Kazakhstan, in 1990. She received the B.Eng. and M.Sc. degrees in electrical and electronic engineering, and the Ph.D. degree in science, engineering, and technology from Nazarbayev University, Astana, Kazakhstan, in 2015, 2017, and 2022, respectively. Her Ph.D. dissertation was focused over the development of machine learning based classification technique for power and distribution transformers diagnostic. Prior to Ph.D. studies, she was a Manufacturing Engineer with "Granit-Thales Electronics" LLP in Almaty, Kazakhstan, in 2017, where she was responsible for manufacture, testing and optimization of radar station. She is currently a Postdoctoral Researcher with the School of Engineering and Digital Sciences, Nazarbayev University. Her research interests include power systems, high voltage equipment testing, transformer diagnostics, machine learning application in power system, overhead line insulator fault detection, and renewable energy sources.

GEVORK B. GHAREHPETIAN (Senior Member, IEEE) received the B.S. degree (Hons.) in electrical engineering from Tabriz University, Tabriz, Iran, in 1987, the M.S. degree (Hons.) in electrical engineering from the Amirkabir University of Technology (AUT), Tehran, Iran, in 1989, and the Ph.D. degree (Hons.) in electrical engineering from Tehran University, Tehran, in 1996.

In his Ph.D. studies, he has received a Scholarship from German Academic Exchange Service (DAAD), from 1993 to 1996. He was with High Voltage Institute of RWTH Aachen, Aachen, Germany. He was holding an assistant professor position with AUT, from 1997 to 2003, the position of an Associate Professor, from 2004 to 2007, and has been a Professor, since 2007.

Dr. Gharehpetian was selected by the Ministry of Science Research and Technology (MSRT) as the Distinguished Professor of Iran, by Iranian Association of Electrical and Electronics Engineers (IAEEE) as the Distinguished Researcher of Iran, by Iran Energy Association (IEA) as the Best Researcher of Iran in the field of energy, by the MSRT as the Distinguished Researcher of Iran, by the Academy of Science of the Islamic Republic of Iran as the Distinguished Professor of electrical engineering, by National Elites Foundation as the Laureate of Alameh Tabatabaei Award, by National Elites Foundation as the Laureate of Sheikh Mofid Award, and was awarded the National Prize, in 2008, 2010, 2018, 2018, 2019, 2019, and 2024, respectively. Based on the Web of Science database, from 2005 to 2023, he is among world's top 1% elite scientists according to Essential Science Indicators (ESI) ranking system.

MEHDI BAGHERI (Senior Member, IEEE) received the Ph.D. degree in electrical power engineering and energy systems from the University of New South Wales (UNSW), Sydney, Australia, in 2014.

He was with the Electric Machinery and Drive Laboratory, Electrical Engineering Department, National University of Singapore (NUS), and closely involved with the Rolls-Royce Pte. Ltd., on a Joint Project. Since 2016, he has been with Nazarbayev University, where he is currently an Associate Professor with the Department of Electrical and Computer Engineering. He is the Head of the Smart Energy Systems Laboratory. He is actively involved in the advanced testing of industrial projects, and he provides technical support to multinational companies, specializing in power product manufacturing, strategic relationships between industry and academia, energy management, smart monitoring of power equipment, and analysis and development of sustainable energy systems. His research interests include climate change and energy security, high voltage engineering, wireless power transfer, condition monitoring and assessment, diagnosis of energy equipment in the field, space, marine applications, electrical rotating machines, electrical insulation, power quality, and smart energy systems. He was a member of the National Research Council of Kazakhstan, from 2020 to 2023. He is a member of IEEE PES, IES, and DEIS. In recognition of his contributions to engineering, he received the Scopus Award, in 2022, and in recognition of his distinguished contribution to Kazakhstan science and education, he received the ''Enbegi Ushin Medal'' from Kazakhstan Ministry of Science and Education, in 2024. He is an Associate Editor of IEEE Access and *Frontiers in Energy Research*.